This article has been accepted for publication in a future issue of this journal, but has not been fully edited. Content may change prior to final publication. Citation information: DOI 10.1109/TUFFC.2018.2821440, IEEE Transactions on Ultrasonics, Ferroelectrics, and Frequency Control

Hyperelastic Tuning of One Dimensional Phononic Band-Gaps Using Directional Stress

Andriejus Demčenko, Michael Mazilu, Rab Wilson, Arno W. F. Volker and Jonathan M. Cooper

***Abstract*—In this paper we show that acoustoelasticity in hyperelastic materials can be understood using the framework of non-linear wave mixing, which, when coupled with an induced static stress, leads to a change in the phase velocity of the propagating wave with no change in frequency. By performing Floquet wave eigenvalue analysis, we also show that band-gaps for periodic composites, acting as 1D phononic crystals, can be tuned using this static stress. In the presence of second order elastic nonlinearities, the phase velocity of propagating waves in the phononic structure changes, leading to observable shifts in the band-gaps. Finally, we present numerical examples as evidence that the band-gaps are tuned by both the direction of the stress and its magnitude.**

***Index Terms*—Hyperelasticity, phononic crystals, non-linear ultrasound, Floquet waves.**

I. Introduction

MULTILAYERED periodic composites can be represented as 1D phononic crystals [1], [2], comprising heterogeneous arrays of materials with different elastic properties. Such composites are increasingly being used in the automotive, marine and aerospace industries as load bearing structures. For example, metal-polymer layered structures are now used in the fuselage of aircraft [3]. Similarly in the semiconductor industry, multilayered microstructures with different lattice spacing or thermal expansion coefficient mismatch that will induce differential stresses either during manufacture or in service. The lifetime and performance of such structures will depend upon the applied and, or the residual static stresses, induced either during their manufacture [4] and, or during their operation [5]. The detection of unwanted static stress states is key in determining the risk of failure in many of these safety-critical structures [6] as this may lead to the propagation of defects [7], which will ultimately affect their structural or functional performance.

Composite structures can be represented as 1D phononic crystals, which can contain measurable band-gaps [8] for ultrasonic waves. The spectral features of the ultrasound after interacting with the phononic structure will represent characteristics of its inherent periodic structure. Thus, when composite structures experience an applied or residual static stress, the ultrasonic wave propagation velocities will change within the different layers, as the characteristic of the band-gap changes.

In this work, starting from the non-linear equations of motion [9], we deduce the dispersion relationships in such 1D phononic structures in the presence of the static stress, which can be described as a zero frequency wave [10]. These equations allow us to interpret the phenomena of acoustoelasticity in terms of a non-linear wave-mixing process [9] between a propagating wave and a zero frequency wave. During this mixing the output frequency does not shift but the phase velocity of the propagating wave changes. The effect is enhanced by the presence of periodicity within the composite (which acts as a 1D phononic crystal). As a consequence of the interplay between the phononic crystal and the ultrsonic non-linear response to the static stress, the effect becomes observable, and indeed provides a method of characterising changes in the composite.

Using this principle, we now develop a new model to enable us to analyze how the composite, represented as a band-gap in a 1D phononic crystal, depends upon the applied static stress. Our analysis is underpinned by using non-linear wave mixing [9] together with a recently revised acoustoelasticity theory in biaxially stressed hyperelastic plate-like structures [11] and Floquet (Floquet-Bloch) wave theory for an infinite periodic medium [12].

Using this understanding of band-gaps in composites potentially introduces an important new method for structural health monitoring. The fact that the band-gaps can be controlled actively by the application of a static stress may also, in the future, lead to development of stress sensitive metamaterials [13]. In order to implement this concept, we used a recursive stiffness matrix method [14] to calculate the Floquet wavenumbers and reflection coefficients from a periodic semi-space. Despite the acoustoelastic effect being small [15], numerical analysis shows that the band-gaps were very sensitive both to the static stress direction and to its magnitude – thus showing the potential of this method to detect defects in periodic composites. The model was also validated using data from the previously reported works [11], [16] and these results are presented in Appendix A.

II. Method

The non-linear equation of motion for an ideal isotropic solid is given by [9]:

$$\rho\frac{\partial^2 v_i}{\partial t^2} - \mu\frac{\partial^2 v_i}{\partial x_j \partial x_j} - (\lambda+\mu)\frac{\partial^2 v_j}{\partial x_i \partial x_j} = \frac{\partial \sigma_{ij}}{\partial x_j}, \qquad (1)$$

A. Demčenko, R. Wilson and J. M. Cooper are with Division of Biomedical Engineering, School of Engineering, Rankine Building, Oakfield Avenue,The University of Glasgow, Glasgow, G12 8LT, UK e-mail: andriejus.demcenko@glasgow.ac.uk

M. Mazilu is with the SUPA, School of Physics and Astronomy, University of St Andrews, St Andrews, KY16 9SS, UK.

A. W. F. Volker is with the Acoustics and Sonar, TNO, Oude Waalsdorperweg 63, 2597 AK Den Haag, The Netherlands.

Manuscript received October XX, 2017; revised October XX, 2017.

This article has been accepted for publication in a future issue of this journal, but has not been fully edited. Content may change prior to final publication. Citation information: DOI 10.1109/TUFFC.2018.2821440, IEEE Transactions on Ultrasonics, Ferroelectrics, and Frequency Control

where ρ is the density of the undeformed medium, $\mathbf{v}$ is the displacement vector in the solid, $x_1 = x$, $x_2 = y$, $x_3 = z$, t are the space and time coordinates and λ, μ are the Lamé constants. We use here the summation over repeated indices convention. The left hand side corresponds to the linear wave equation and the right hand side to the divergence of the non-linear stress tensor given by:

$$\begin{aligned}\sigma_{ij}(\mathbf{v}) &= (\mu + A/4)\left(\frac{\partial v_s}{\partial x_i}\frac{\partial v_s}{\partial x_j} + \frac{\partial v_i}{\partial x_s}\frac{\partial v_j}{\partial x_s} + \frac{\partial v_i}{\partial x_s}\frac{\partial v_s}{\partial x_j}\right) \\ &+ \frac{A}{4}\frac{\partial v_s}{\partial x_i}\frac{\partial v_j}{\partial x_s} + C\frac{\partial v_s}{\partial x_s}\frac{\partial v_r}{\partial x_r}\delta_{ij} \\ &+ \frac{B+\lambda}{2}\left(\frac{\partial v_s}{\partial x_r}\frac{\partial v_s}{\partial x_r}\delta_{ij} + 2\frac{\partial v_i}{\partial x_j}\frac{\partial v_s}{\partial x_s}\right) \\ &+ \frac{B}{2}\left(\frac{\partial v_s}{\partial x_r}\frac{\partial v_r}{\partial x_s}\delta_{ij} + 2\frac{\partial v_j}{\partial x_i}\frac{\partial v_s}{\partial x_s}\right), \qquad (2)\end{aligned}$$

where A, B and C are the third order elastic constants in Landau and Lifshitz notation [17].

In order to model the non-linear interaction between the static strain and an ultrasonic wave we consider:

$$\mathbf{v} = \mathbf{e}\cdot\mathbf{r} + \mathbf{u}e^{-\mathrm{i}(\omega t - \mathbf{k}\cdot\mathbf{r})} \qquad (3)$$

where $\mathbf{e}$ is a diagonal static strain tensor with the terms (e_{11}, e_{22}, e_{33}) on the diagonal. Using Eq. (1) and Eq. (2) we define a modified dispersion relationship linking the static strain to the phase velocity for a wave propagating in the x_1 direction (detailed calculations are presented in these results are presented in Appendix B)

$$\begin{aligned}\rho c_L^2 &= 2Ae_{11} + (2B+\lambda)(3e_{11} + e_{22} + e_{33}) \\ &\quad +2C(e_{11} + e_{22} + e_{33}) + 6e_{11}\mu + \rho c_{0L}^2, \qquad (4) \\ \rho c_S^2 &= (A/2 + 2\mu)(e_{11} + e_S) \\ &\quad +(B+\lambda)(e_{11} + e_{22} + e_{33}) + \rho c_{0S}^2, \qquad (5)\end{aligned}$$

where the subscript S corresponding to the shear wave is either 22 or 33, and c_{0L} and c_{0S} are the longitudinal and shear wave velocities respectively in the unstressed medium. We show that non-linear wave mixing and the induction of static stress leads to an effective change in the phase velocity of the propagating wave with a zero-frequency shift [10]. We note that propagation along different directions or non-diagonal stress tensors can also be deduced in a similar manner, however the dispersion relations (4) and (5) will contain more terms and the stressed media will show anisotropic properties.

To analyze the elastic wave propagation in these hyperelastic 1D phononic crystals, we implement a recursive stiffness matrix method. The Floquet wave equation is given by [14]:

$$\begin{aligned}A_3\cos(3k_{z\mathrm{F}}H) &+ A_2\cos(2k_{z\mathrm{F}}H) \\ &+ A_1\cos(k_{z\mathrm{F}}H) + A_0 = 0, \qquad (6)\end{aligned}$$

where $k_{z\mathrm{F}}$ is the vertical Floquet wavenumber and H is the unit cell thickness, Fig. 1. The Floquet wave coefficients A_i are given below (these have been modified and updated from those originally reported [18]) in terms of the unit cell stiffness matrix:

$$A_3 = |\mathbf{K}_{\mathrm{c}}^{21}|, \qquad (7)$$

$$A_2 = 1/2(|\mathbf{M} + \mathbf{K}_{\mathrm{c}}^{21}| + |\mathbf{M} - \mathbf{K}_{\mathrm{c}}^{21}|) - |\mathbf{M}|, \qquad (8)$$

$$\begin{aligned}A_1 &= 1/2(|\mathbf{M} + \mathbf{K}_{\mathrm{c}}^{21}| - |\mathbf{M} + \mathbf{K}_{\mathrm{c}}^{12}| \\ &+ |\mathbf{K}_{\mathrm{c}}^{21} - \mathbf{K}_{\mathrm{c}}^{12}|) - 2|\mathbf{K}_{\mathrm{c}}^{21}|, \qquad (9)\end{aligned}$$

$$\begin{aligned}A_0 &= 1/2(|\mathbf{M} + \mathbf{K}_{\mathrm{c}}^{12} - \mathbf{K}_{\mathrm{c}}^{21}| \\ &+ |\mathbf{M} - \mathbf{K}_{\mathrm{c}}^{12} + \mathbf{K}_{\mathrm{c}}^{21}|) - 2A_2, \qquad (10)\end{aligned}$$

where $\mathbf{M}$=$\mathbf{K}_{\mathrm{c}}^{22} - \mathbf{K}_{\mathrm{c}}^{11}$, $|\mathbf{M}|$ is the determinant of matrix $\mathbf{M}$, $\mathbf{K}_{\mathrm{c}}$ is the whole stiffness matrix of the unit periodic cell [14]. The amplitude reflection coefficient from a submersed semi-space in terms of the Floquet wave equation parameters [19] can thus be written in the following form:

$$\mathrm{R_{as}} = \frac{S_{\mathrm{F}}^{33} - \cos\theta/(i\omega\rho_{\mathrm{f}}c_{\mathrm{f}})}{S_{\mathrm{F}}^{33} + \cos\theta/(i\omega\rho_{\mathrm{f}}c_{\mathrm{f}})}, \qquad (11)$$

where θ is the wave incidence angle, Fig. 1, $\omega = 2\pi f$, f is the wave frequency, ρ_{f} is the volumetric mass density, c_{f} is the wave speed. S_{F}^{33} is the $(3,3)$ element in the 3×3 surface compliance matrix for a homogeneous or layered anisotropic semi-space.

As an example of a 1D phononic crystal, see Fig. 1, we now show results for a two layered unit cell of the metal polymer periodic medium containing an aluminum and a polyvinylchloride (PVC) layer of 0.1 mm thickness. The following second order elastic material properties were used in the eigenvalue analysis of the Floquet waves in the 1D hyperelastic phononic structure: $\lambda_1 = 54.307$ GPa, $\mu_1 = 27.174$ GPa, $\rho_1 = 2704$ kg/m^3 and $\lambda_2 = 3.8745$ GPa, $\mu_2 = 1.6335$ GPa, $\rho_2 = 1350$ kg/m^3 for the aluminum and PVC layers, respectively [11], [9]. The corresponding third order elastic constants are, in Murnaghans notation, [20]: $l_1 = -281.5$ GPa, $m_1 = -339$ GPa, $n_1 = -416$ GPa and $l_2 = -33.43$ GPa, $m_2 = -20.88$ GPa, $n_2 = -15.86$ GPa.

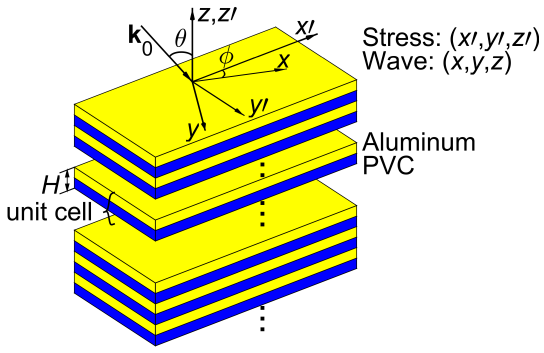

Fig. 1: Two-layered unit cell of the periodic medium and coordinate system for the static stress and wave propagation directions. $\mathbf{k}_0$ is the incident wave and θ is the wave incidence angle from the fluid. The stress is specified in the primed coordinate system and guided waves propagate along x direction at any arbitrary angle ϕ from x' direction. The analysis is conducted in the unprimed coordinate system (x, y, z) hence the primed coordinate system is rotated through the angle ϕ. The coordinate system is selected so that the xz plane coincides with the wave incident plane, hence $k_y = 0$.

This article has been accepted for publication in a future issue of this journal, but has not been fully edited. Content may change prior to final publication. Citation information: DOI 10.1109/TUFFC.2018.2821440, IEEE Transactions on Ultrasonics, Ferroelectrics, and Frequency Control

The relationships between the third order elastic constants in Landau and Lifshitz and Murnaghan's notations are given in Appendix C. The above semi-space fluid properties are $c_{\mathrm{f}} = 1480$ m/s and $\rho_{\mathrm{f}} = 1000\ \mathrm{kg/m^3}$.

III. Results

In our analysis three scenarios were investigated, namely: (i) using an applied static stress σ_{22}, which is constant and equal to 200 MPa (tensile case) but where we vary both the angle ϕ (see Fig. 1) in the range $0^\circ - 90^\circ$ with 1° increments and the incident wave frequency f in the range 0 to 20.0 MHz with 1 kHz increments (this scenario corresponds to $\phi - f$ plane); (ii) using an angle ϕ which is constant and equal to 90°, but where we vary both the stress σ_{22} in the range -200 MPa $+200$ MPa with 4.35 MPa increments and the incident wave frequency varies in the range 0 to 20.0 MHz, with 1 kHz increments (this scenario corresponds to $\sigma - f$ plane); and finally, (iii) the scenario where the frequency of the incidence wave is kept constant and equal to 20 MHz, and where we vary both the angle ϕ in the range $0^\circ - 90^\circ$ and the stress σ_{22} in the range -200 MPa $+200$ MPa (the last scenario corresponds to $\sigma - \phi$ plane).

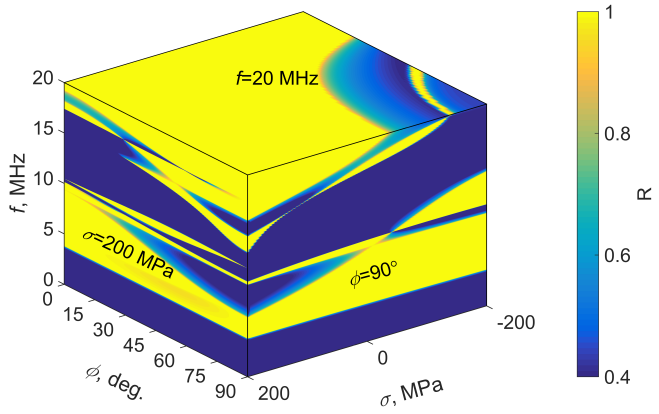

Fig. 2: Band-gaps in the periodic semi-space loaded by fluid when the wave incidence angle $\theta = 35^\circ$. $\mathrm{R} = 1$ and $\mathrm{R} < 1$ zones correspond to stop and pass-bands, respectively.

Figure 2 shows the subsequent 3D plot of the energy reflection coefficient from the fluid loaded statically stressed periodic semi-space. In all three scenarios, the wave incidence angle was $\theta = 35^\circ$ (to provide a representative illustration of the influence of the acoustoelastic effect on band-gaps in the periodic semi-space). We used a static stress limit of ± 200 MPa which can be either be an applied or residual stress within the structure [21].

For band-gaps which correspond to zones where $\mathrm{R} = 1$, pass-bands are formed where $\mathrm{R} < 1$. The results also show that the band-gaps have a strong dependence (band-gap becomes 2.5 times narrower due to the stress) on the static stress and the wave propagation direction ϕ (Fig. 1) in the periodic semi-space ($\phi - f$ plane). The band-gaps depend significantly on the stress value when $\phi = 90^\circ$, see plane $\sigma - f$ in Fig. 2.

When $\sigma = 0$ MPa, the energy reflection coefficient corresponds to the unstressed semi-space case. When the incidence wave frequency f is equal to 20.0 MHz, plane $\sigma - \phi$, the results also show that a band-gap is formed in a wide range of the parameters σ and ϕ. The results are presented in more detail below for the second scenario (ii), which demonstrates the corresponding response for compression and tensile stress case in $\phi - f$ plane.

Following on from this, we represent the ultrasonic wave response of the periodic structure in terms of Floquet wavenumbers, where the unit cell thickness product $\Re(k_{z\mathrm{F}} \times H)$ and energy reflection coefficients R from a periodic semi-space loaded by a fluid when the angle $\phi = 90^\circ, 45^\circ, 0^\circ$, see Fig. 1. Two separate cases are considered in the analysis with respect to the angle ϕ, namely when the shear horizontal wave motion is not coupled to the sagittal wave motion (Figs. 3a-c and Figs. 3g-i), and secondly, when coupling occurs between the shear horizontal and sagittal wave motions [22] (Figs. 3d-f). In the reference case, where $\sigma_{22} = 0$ MPa and $\mathrm{m}_{\mathrm{o},i}$, $\mathrm{m}_{\mathrm{i},j}$ denote the out-of-plane shear wave and in-plane shear and longitudinal wave modes respectively. Modes in both compressive and tensile cases are denoted $\mathrm{n}_{\mathrm{o},i}$, $\mathrm{n}_{\mathrm{i},j}$. For the reference case, the 1D phononic crystal contains 3 well-defined zones (see Fig. 3a) comprising an effective homogeneous medium from 0 - 3.7 MHz, (see Fig. 3b, mode $\mathrm{m}_{\mathrm{i}1}$); the first band-gap in the frequency range 3.7 - 9.1 MHz, and finally, the main pass-band in the frequency range 10.0 - 17.1 MHz.

When the static stress direction is coincident with the wave propagation direction ($\phi = 90^\circ$), Figs. 3a-c, significant changes occur in the band-gap zones of the phononic crystal, despite the shear wave motion being decoupled from the sagittal wave motion. In this case, however, the first band-gap is almost unaffected in the compression stress. However, in the tensile case, this band-gap reduces from 3.7 MHz - 9.1 MHz to 3.8 MHz - 5.9 MHz becoming 2.5 times narrower. This is due to a change in the mode dispersion of the structure as shown in Fig. 3b of the stressed mode $\mathrm{n}_{\mathrm{i}2}$ with respect to the same reference mode $\mathrm{m}_{\mathrm{i}2}$. The tensile static stress, Fig. 3c, also shifts down the second band-gap which occurs in the frequency range 12.4 MHz - 13.9 MHz, see the modes $\mathrm{m}_{\mathrm{i}3}$, $\mathrm{m}_{\mathrm{i}4}$ and $\mathrm{n}_{\mathrm{i}3}$, $\mathrm{n}_{\mathrm{i}4}$. The compression stress, Fig. 3a, causes a significant band-gap shift in the frequency range 10 MHz to 13.3 MHz, this is shown in Fig. 3b where the reference mode $\mathrm{m}_{\mathrm{i}3}$ is shifted up, but the dispersion remains unchanged, whereas the $\mathrm{m}_{\mathrm{i}2}$ mode does not shift significantly but its dispersion is changed. The out-of plane modes $\mathrm{m}_{\mathrm{o},i}$ are relatively insensitive to the applied stress in comparison with the $\mathrm{m}_{\mathrm{i},j}$ modes.

In the case of the $\mathrm{m}_{\mathrm{i},j}$ modes, the results show that the smallest difference in ultrasonic response from the stressed periodic structures is observed when the wave propagation and stress directions are orthogonal ($\phi = 0^\circ$), see Figs. 3g-i. In this case the $\mathrm{m}_{\mathrm{o},i}$ modes are sensitive to the applied stress and these modes are consequently significantly shifted (see the modes $\mathrm{n}_{\mathrm{o}2}$ and $\mathrm{n}_{\mathrm{o}3}$).

Finally, when the angle $\phi = 0^\circ$ or $\phi = 90^\circ$ the modes present in the structure are pure. However, when the angle ϕ deviates from these values, the modes no longer remain pure and the shear horizontal wave motion couples into the sagittal

This article has been accepted for publication in a future issue of this journal, but has not been fully edited. Content may change prior to final publication. Citation information: DOI 10.1109/TUFFC.2018.2821440, IEEE Transactions on Ultrasonics, Ferroelectrics, and Frequency Control

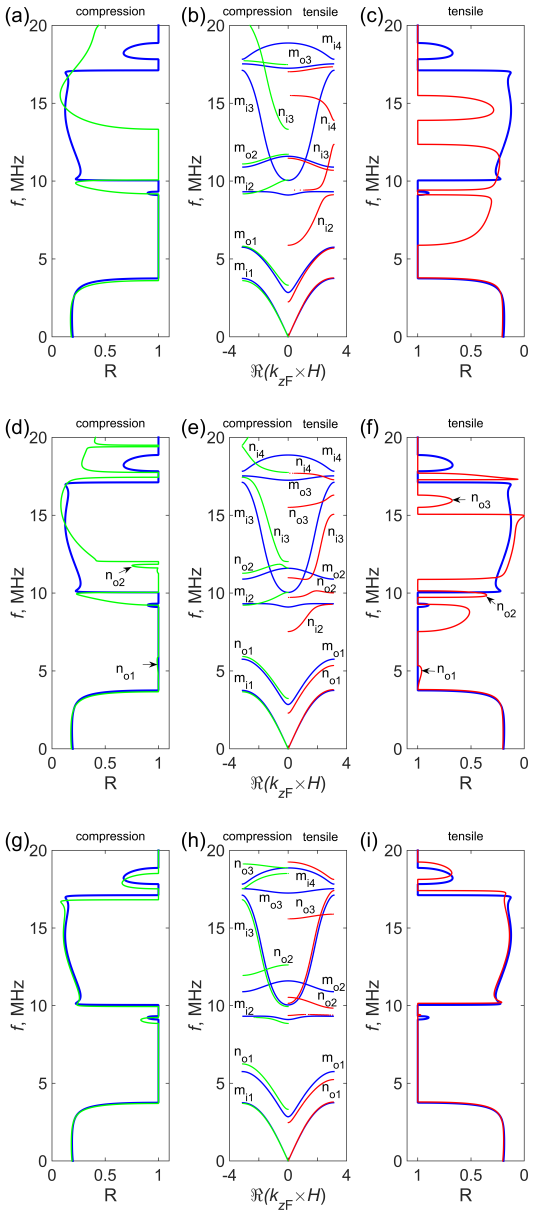

Fig. 3: Ultrasonic response from a periodic semi-space loaded by fluid when the incident beam angle $\theta = 35°$ and angle ϕ is: $\phi = 90°$ (a)-(c), $\phi = 45°$ (d)-(f), and $\phi = 0°$ (g)-(i). (a), (d), (g) and (c), (f), (i) show the energy reflection coefficients for the compression and tensile stress cases, respectively. The corresponding Floquet wavenumber and unit cell thickness product $\Re(k_{zF} \times H)$ is depicted in (b), (e) and (h). Blue curves show the reference case when $\sigma_{22} = 0$ MPa whilst green and red curves show the response when $\sigma_{22} = -200$ MPa and $\sigma_{22} = 200$ MPa, respectively.

wave motion. For example, this coupling is shown for the case when $\phi = 45°$ in the reflection coefficient, for the frequency range 3.8 - 5.3 MHz (Fig. 3f, mode $\mathrm{n_{o1}}$) in the tensile stress case (where weaker coupling is observed in the compression stress case). The modes $\mathrm{n_{o2}}$ and $\mathrm{n_{o3}}$ have a higher coupling to the sagittal wave motion. In the compression stress case (Fig. 3d) the first band-gap is less affected than in the tensile stress case. The results show that in the tensile stress case the first band-gap is formed in the frequency range 5.3 - 7.5 MHz, and it is 2.5 narrower compared with the band-gap when $\sigma_{22} = 0$ (see Fig. 3f). The narrowing is caused by a change in the $\mathrm{m_{i2}}$ reference mode dispersion, see $\mathrm{n_{i2}}$. The main pass-band is also narrower as is seen in the frequency ranges 12.0 - 17.4 MHz and 10.9 - 15.0 MHz for the compression and tensile stress cases, respectively. These latter changes occur due to the $\mathrm{m_{i3}}$ mode shifting up in case of compression stress, and shifting down in case of tensile stress, see the mode $\mathrm{n_{i3}}$.

IV. Conclusion

In conclusion, we show that static stress together with second-order material non-linearities have a significant influence on the band-gaps in 1D phononic crystals. This acoustoelastic effect can be understood as the non-linear wave mixing between a zero frequency wave and a propagating wave. Our results extend recently reported work [13] where analysis was conducted using small amplitude motions in a normal direction, while we now consider finite amplitude elastic waves having oblique angle propagation.

We show that the band-gaps are highly tunable with respect to the direction and the magnitude of static stress. We also show that the effect is enhanced both by the resonances in the 1D phononic crystals and by the coupling between the shear horizontal and sagittal wave. In future, our study has the potential to enable a number applications in industries using periodic composites structures, including the integrity of large-scale composite structures used in the aerospace industry or of stresses caused by thermal mismatches in microstructures created within the semiconductor industry.

Appendix A
Validation of the Implementation of the Stiffness Matrix Method for Guided and Floquet Waves in Layered Structures

Figure 4 shows the Lamb wave phase velocity dependence for three modes, two of which are symmetric $\mathrm{s_0}$, $\mathrm{s_1}$ and one, which is antisymmetric $\mathrm{a_1}$, with respect to the angle ϕ in a single-layered aluminum plate when applied stress $\sigma_{11} = 57.5$ MPa. The material properties are listed in Ref. [11]. Our results, carried out as replicates, show an excellent agreement with the reported results in Ref. [11], see Fig. 10.

Figure 5 also shows Floquet wavenumbers for the two-layered viscoelastic unit cell comprising aluminum and epoxy layers of equal thickness. The incidence angle of longitudinal wave in nylon is 80°. The material properties are listed in [16]. Our results show an excellent agreement with the reported results in Ref. [16], see Fig. 2(b).

Appendix B
Static Strain Dispersion Relations

Using the ultrasonic wave and static strain superposition defined by (3) we can determine separately the linear and non-linear effects in equation of motion (1). To simplify the notations, we consider the longitudinal and shear waves

This article has been accepted for publication in a future issue of this journal, but has not been fully edited. Content may change prior to final publication. Citation information: DOI 10.1109/TUFFC.2018.2821440, IEEE Transactions on Ultrasonics, Ferroelectrics, and Frequency Control

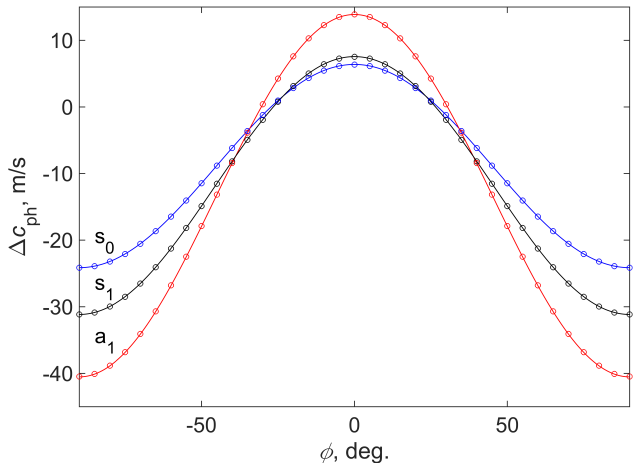

Fig. 4: Lamb wave phase velocity dependence on the angle ϕ in aluminum plate of thickness 6.35 mm when $\sigma_{11} = 57.5$ MPa, where circles indicate the reported data from Ref. [11]. Calculations are performed at the following frequencies: 0.25 MHz (s_0 mode), 0.4 MHz (a_1 mode) and 0.6 MHz (s_1 mode).

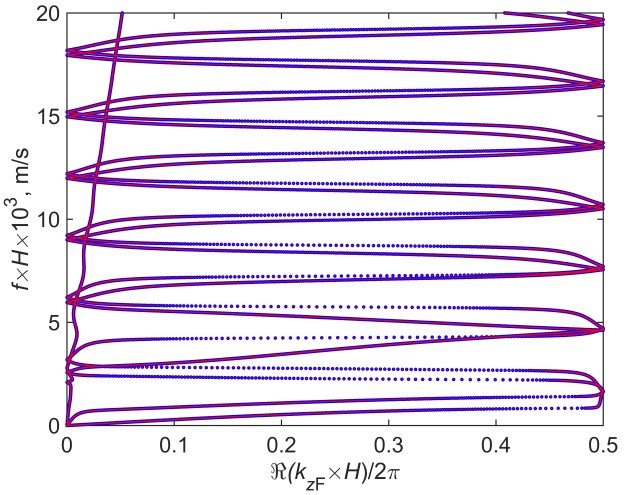

Fig. 5: Relation between $\Re(k_{z\mathrm{F}} \times H)$ and $f \times H$, where red color indicates the data from Ref. [16]. The viscoelastic unit cell comprises aluminum and epoxy of equal thickness. The incidence angle is 80° corresponding to longitudinal wave in nylon.

separately. In the case of longitudinal waves propagating in the x_1 direction, we have the linear part equal to

$$\rho\frac{\partial^2 v_i}{\partial t^2} - \mu\frac{\partial^2 v_i}{\partial x_j \partial x_j} - (\lambda+\mu)\frac{\partial^2 v_j}{\partial x_i \partial x_j} = u_i e^{-\mathrm{i}(\omega t - \mathbf{k}\cdot\mathbf{r})} k^2(\lambda + 2\mu - \rho c_{0L}^2) \quad (12)$$

where the polarisation amplitude $\mathbf{u}$ is parallel to the wave-vector $\mathbf{k}$. Similarly, we can determine the non-linear stress tensor for the superposition (3)

$$\frac{\partial \sigma_{ij}}{\partial x_j} = -u_i e^{-\mathrm{i}(\omega t - \mathbf{k}\cdot\mathbf{r})} k^2 (2C(e_{11}+e_{22}+e_{33}) + 2Ae_{11} + (2B+\lambda)(3e_{11}+e_{22}+e_{33}) + 6e_{11}\mu) \quad (13)$$

Equating these two equations (12) and (13) allows us to introduce a new static strain dependent wave velocity c_{0L} as defined by equation (4). The wave part of the superposition is then a solution of the linear wave equation taking this modified velocity into account.

In the same way, we proceed to evaluate the effect of the static strain on shear waves. In this case, the linear linear part of the wave equation evaluates to:

$$\rho\frac{\partial^2 v_i}{\partial t^2} - \mu\frac{\partial^2 v_i}{\partial x_j \partial x_j} - (\lambda+\mu)\frac{\partial^2 v_j}{\partial x_i \partial x_j} = u_i e^{-\mathrm{i}(\omega t - \mathbf{k}\cdot\mathbf{r})} k^2(\mu - \rho c_{0S}^2) \quad (14)$$

where the polarisation amplitude $\mathbf{u}$ is perpendicular to the wave-vector $\mathbf{k}$. The non-linear stress tensor for the superposition (3) in this case is equal to:

$$\frac{\partial \sigma_{ij}}{\partial x_j} = -u_i e^{-\mathrm{i}(\omega t - \mathbf{k}\cdot\mathbf{r})} k^2 (A/2 + 2\mu)(e_{11}+e_S) + (B+\lambda)(e_{11}+e_{22}+e_{33}) \quad (15)$$

where the subscript S corresponding to the shear wave direction with indices equal to either 22 or 33. Similarly to the longitudinal case, equating (14) and (15) allows us to introduce a new static strain dependent wave velocity c_{0S} as defined by equation (5). The wave part of the superposition is then a solution of the linear wave equation taking this modified velocity into account.

Appendix C
The relationship between third order elastic constants for isotropic solids

The relationships between the third order elastic constants in Landau and Lifshitz (A, B and C) and Murnaghan's notations are given by:

$$l = B + C, m = A/2 + B, n = A, \quad (16)$$

where l, m and n are the third order elastic constants in Murnaghan's notations.

Acknowledgment

Authors acknowledge Dr. Jennifer Michaels from Georgia Tech and Dr. Tan Eng Leong from Nanyang Technological University for providing data used in Figs. 4 and 5. Authors would like to acknowledge Dr. Manlio Tassieri for his helpful discussions. JMC acknowledges EPSRC Fellowship (EP/K027611/1) and the ERC advanced investigator award (340117 - Biophononics).

References

[1] J. H. Page, A. Sukhovich, S. Yang, M. L. Cowan, F. Van Der Biest, A. Tourin, M. Fink, Z. Liu, C. T. Chan, and P. Sheng, "Phononic crystals," *Physica Status Solidi (b)*, vol. 241, no. 15, pp. 3454–3462, Dec. 2004.

[2] Y. Pennec, J. Vasseur, B. Djafari-Rouhani, L. Dobrzyński, and P. Deymier, "Two-dimensional phononic crystals: Examples and applications," *Surface Science Reports*, vol. 65, no. 8, pp. 229–291, 2010.

[3] L. Vogelesang and A. Vlot, "Development of fibre metal laminates for advanced aerospace structures," *Journal of Materials Processing Technology*, vol. 103, no. 1, pp. 1–5, 2000.

[4] S. Khan, R. Alderliesten, and R. Benedictus, "Delamination growth in fibre metal laminates under variable amplitude loading," *Composites Science and Technology*, vol. 69, no. 15-16, pp. 2604–2615, 2009.

[5] P. Peddiraju, J. Noh, J. Whitcomb, and D. Lagoudas, "Prediction of cryogen leak rate through damaged composite laminates," *Journal of Composite Materials*, vol. 41, no. 1, pp. 41–71, 2007.

[6] T. Zhang, Q. Zhu, W. Huang, Z. Xie, and X. Xin, "Stress field and failure probability analysis for the single cell of planar solid oxide fuel cells," *Journal of Power Sources*, vol. 182, no. 2, pp. 540–545, 2008.

[7] A. Evans and J. Hutchinson, "The thermomechanical integrity of thin films and multilayers," *Acta Metallurgica Et Materialia*, vol. 43, no. 7, pp. 2507–2530, 1995.

[8] M. Kushwaha, P. Halevi, L. Dobrzynski, and B. Djafari-Rouhani, "Acoustic band structure of periodic elastic composites," *Physical Review Letters*, vol. 71, no. 13, pp. 2022–2025, 1993.

[9] V. Korneev and A. Demčenko, "Possible second-order nonlinear interactions of plane waves in an elastic solid," *Journal of the Acoustical Society of America*, vol. 135, no. 2, pp. 591–598, 2014.

[10] J. Rivière, L. Pimienta, M. Scuderi, T. Candela, P. Shokouhi, J. Fortin, A. Schubnel, C. Marone, and P. A. Johnson, "Frequency, pressure, and strain dependence of nonlinear elasticity in berea sandstone," *Geophysical Research Letters*, vol. 43, no. 7, pp. 3226–3236, 2016.

[11] N. Gandhi, J. Michaels, and S. Lee, "Acoustoelastic lamb wave propagation in biaxially stressed plates," *Journal of the Acoustical Society of America*, vol. 132, no. 3, pp. 1284–1293, 2012.

[12] A. Braga and G. Herrmann, "Floquet waves in anisotropic periodically layered composites," *Journal of the Acoustical Society of America*, vol. 91, no. 3, pp. 1211–1227, 1992.

[13] P. Galich, N. Fang, M. Boyce, and S. Rudykh, "Elastic wave propagation in finitely deformed layered materials," *Journal of the Mechanics and Physics of Solids*, vol. 98, pp. 390–410, 2017.

[14] S. Rokhlin and L. Wang, "Stable recursive algorithm for elastic wave propagation in layered anisotropic media: Stiffness matrix method," *Journal of the Acoustical Society of America*, vol. 112, no. 3 I, pp. 822–834, 2002.

[15] M. Hamilton and D. Blackstock, *Nonlinear Acoustics*. Academic Press, 1998.

[16] E. L. Tan, "Generalized eigenproblem of hybrid matrix for floquet wave propagation in one-dimensional phononic crystals with solids and fluids," *Ultrasonics*, vol. 50, no. 1, pp. 91–98, 2010.

[17] L. D. Landau & E.M. Lifshitz, *Theory of Elasticity*, 1959.

[18] Y. Ishii and S. Biwa, "Transmission of ultrasonic waves at oblique incidence to composite laminates with spring-type interlayer interfaces," *Journal of the Acoustical Society of America*, vol. 138, no. 5, pp. 2800–2810, 2015.

[19] L. Wang and S. Rokhlin, "Time-resolved line focus acoustic microscopy of layered anisotropic media: Application to composites," *IEEE Transactions on Ultrasonics, Ferroelectrics, and Frequency Control*, vol. 49, no. 9, pp. 1231–1244, 2002.

[20] F. D. Murnaghan, "Finite deformations of an elastic solid," *American Journal of Mathematics*, vol. 59, no. 2, pp. 235–260, 1937.

[21] J. Dike and G. Johnson, "Residual stress determination using acoustoelasticity," *Journal of Applied Mechanics, Transactions ASME*, vol. 57, no. 1, pp. 12–17, 1990.

[22] Y. Li and R. Thompson, "Influence of anisotropy on the dispersion characteristics of guided ultrasonic plate modes," *Journal of the Acoustical Society of America*, vol. 87, no. 5, pp. 1911–1931, 1990.